LETTERS

The velocity of climate change

Scott R. Loarie[1], Philip B. Duffy[1,2], Healy Hamilton[3], Gregory P. Asner[1], Christopher B. Field[1] & David D. Ackerly[4]

The ranges of plants and animals are moving in response to recent changes in climate[1]. As temperatures rise, ecosystems with 'nowhere to go', such as mountains, are considered to be more threatened[2,3]. However, species survival may depend as much on keeping pace with moving climates as the climate's ultimate persistence[4,5]. Here we present a new index of the velocity of temperature change (km yr^{-1}), derived from spatial gradients (°C km^{-1}) and multimodel ensemble forecasts of rates of temperature increase (°C yr^{-1}) in the twenty-first century. This index represents the instantaneous local velocity along Earth's surface needed to maintain constant temperatures, and has a global mean of 0.42 km yr^{-1} (A1B emission scenario). Owing to topographic effects, the velocity of temperature change is lowest in mountainous biomes such as tropical and subtropical coniferous forests (0.08 km yr^{-1}), temperate coniferous forest, and montane grasslands. Velocities are highest in flooded grasslands (1.26 km yr^{-1}), mangroves and deserts. High velocities suggest that the climates of only 8% of global protected areas have residence times exceeding 100 years. Small protected areas exacerbate the problem in Mediterranean-type and temperate coniferous forest biomes. Large protected areas may mitigate the problem in desert biomes. These results indicate management strategies for minimizing biodiversity loss from climate change. Montane landscapes may effectively shelter many species into the next century. Elsewhere, reduced emissions, a much expanded network of protected areas[6], or efforts to increase species movement may be necessary[7].

As climate changes in this century, the current distribution of climatic conditions will be rearranged on the globe; some climates will disappear entirely, and new (no-analogue) climates are expected in wide regions[8]. For species to survive, the persistence of suitable climates is not sufficient. Species must also keep pace with climates as they move[9]. To summarize the speed at which climate is changing, we compute the instantaneous horizontal velocity of temperature change (Fig. 1e) derived from the ratio of temporal (Fig. 1d) and spatial (Fig. 1c) gradients of mean annual near-surface temperature (Fig. 1b) (°C yr^{-1}/°C km^{-1} = km yr^{-1}). As exemplified by California, the spatial gradient of temperature change is greatest on mountain slopes (Fig. 1c): modest displacements in space, moving up or down slope, result in a large change in temperature. As a result, relatively small velocities (Fig. 1e) are required to keep pace with the rate of temperature change (assuming that the climate persists and does not disappear). In contrast, high velocities are required in flatter areas such as California's Central Valley, where large geographic displacements are required to change temperature appreciably.

The magnitude of these results depends on the emissions scenario (Fig. 2a) and also on the period of time over which the temporal gradient is calculated (Fig. 2b). However, velocity patterns of global temperature change are similar across scenarios, with the highest velocities in flat landscapes at higher latitudes (Fig. 2c). Using temperature change calculated from 2000–2100 under the intermediate A1B emissions scenario, the geometric mean velocity was 0.42 km yr^{-1} (0.11–1.46). (Throughout, we summarize uncertainty in the mean by listing upper and lower, ± 1 s.d., estimates in parenthesis.) See Supplementary Fig. 17 for other emissions scenarios. We summarize velocity for biomes of the globe and rank them by increasing mean velocity (Fig. 3). Doing so shows that mountainous biomes require the slowest velocities to keep pace with climate change. In contrast, flatter biomes such as flooded grasslands, mangroves and deserts require much greater velocities. Overall, there is a strong correlation between topographic slope and velocity from temperature change (correlation coefficient = −0.92; see Supplementary Fig. 18).

Land-cover change results in formidable barriers to species movement[10]. Thus, keeping pace with climate change is more feasible in protected areas where landscapes may be less fragmented[11]. The sizes

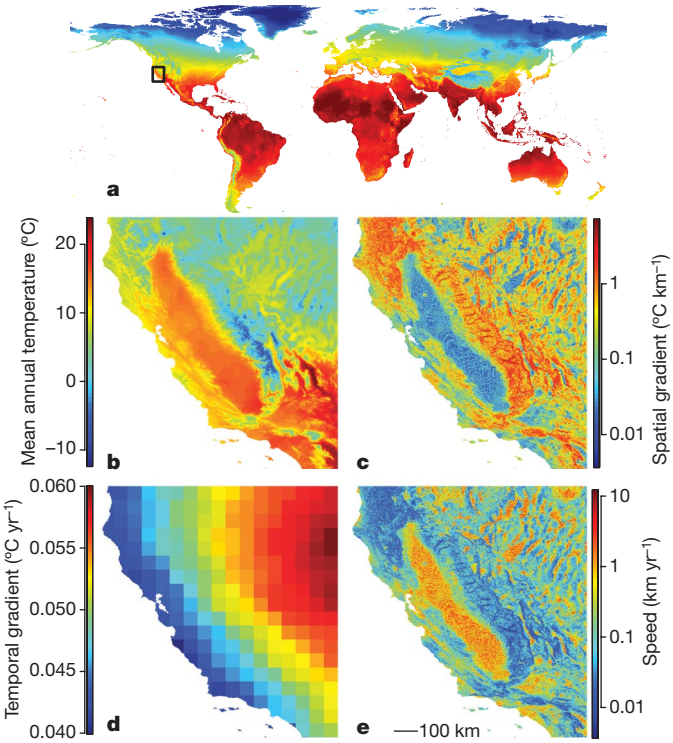

Figure 1 | Changing temperature in California. a, Current (1950–2000) mean annual temperature at 800 m resolution. The black rectangle indicates the Central California inset in **b**. **c**, The spatial gradient of temperature change using a 9 pixel kernel. **d**, The temporal gradient of climate change from 2000–2099 from 0.5 °C 16 general circulation model (GCM) ensemble projection with A1B emissions. **e**, The velocity of climate change determined from the quotient of **d** and **c**.

[1]Carnegie Institution for Science, Department of Global Ecology, Stanford, California 94305, USA. [2]Climate Central, Inc., Palo Alto, California 94301, USA. [3]Center for Applied Biodiversity Informatics, California Academy of Sciences, San Francisco, California 94118, USA. [4]Department of Integrative Biology, University of California, Berkeley, California 94720, USA.

©2009 Macmillan Publishers Limited. All rights reserved

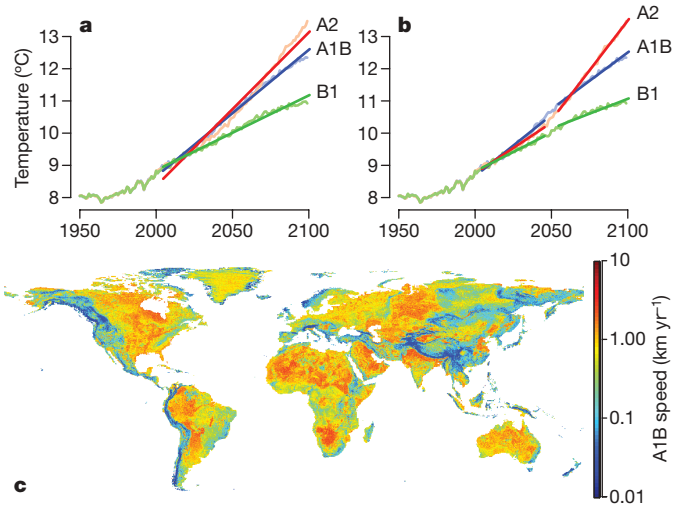

Figure 2 | The velocity of temperature change globally. **a**, Temporal gradients calculated from 2000–2100 across three emissions scenarios (A2, A1B and B1). **b**, Temporal gradients calculated from 2000–2050 and 2050–2100 across three emissions scenarios. Trends plotted here are the average of the global land surface. **c**, A global map of climate velocity calculated using the 2050–2100 Special Report on Emissions Scenarios (SRES) A1B emissions scenario temporal gradient.

of protected areas vary greatly across biomes (see Supplementary Fig. 20). To explore the interaction between protected area sizes and velocities required to keep pace with climate change, we calculated residence times, defined as the diameter of each protected area divided by velocity (km/km yr^{-1} = yr). Assuming that protected areas are circular and disconnected, this index can be interpreted as the time for current climate to cross a protected area. Such residence times exceed 100 years for only 8.02% (2.67–16.49) of protected areas. Figure 4 summarizes these data by biome, ordered by decreasing residence time. The order of residence times is generally the inverse of velocities, across biomes. For example, the three biomes with the slowest velocities have among the four longest residence times. There are also notable differences. For example, the limited size of protected areas in Mediterranean-type, temperate broadleaf and coniferous forest biomes decreases the residence time in these biomes despite relatively low velocities. The rank of these biomes increased from 4, 7 and 2 to 11, 13 and 8 when arranged by decreasing mean residence time (Fig. 4) as opposed to increasing mean velocity (Fig. 3). In contrast, larger protected areas in other biomes decreased their rank despite high velocities of temperature change. For example, the deserts decreased in rank from 12 to 6.

To guide the interpretation of these results, we make three clarifications. First, climate change involves complex interactions among temperature, precipitation and seasonal and historic variability. We focus on mean annual temperature for several reasons. Mean annual temperature is a useful summary of both historic and projected climate change. The direction and magnitude of temperature change is much less uncertain than precipitation change[12]. Growing numbers of examples document the latitudes and elevations of species distributions responding as expected to changing temperatures[13–16]. We repeated all analyses with precipitation (see Supplementary Fig. 19). Interestingly, precipitation spatial gradients are also greatest in mountainous areas due to the influence of rain shadows and orographic effects. As a result the mean velocity, 0.22 km yr^{-1} (0.08–1.90), and overall patterns are similar to those derived by temperature.

Second, there is uncertainty in both the spatial and temporal gradients of climate change. We estimated uncertainty in both of these contributing factors and propagated them through to lower and upper estimates of velocity and residence time (see Supplementary

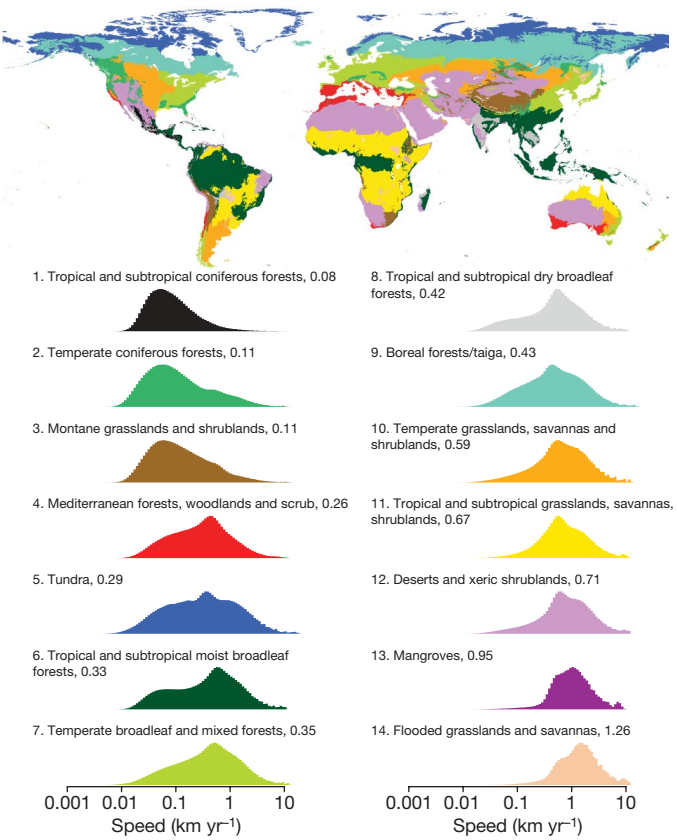

Figure 3 | The velocity of temperature change by biome. A map of biomes and histograms of the speed of temperature change within each biome. Histograms are ordered by increasing velocity according to their geometric means.

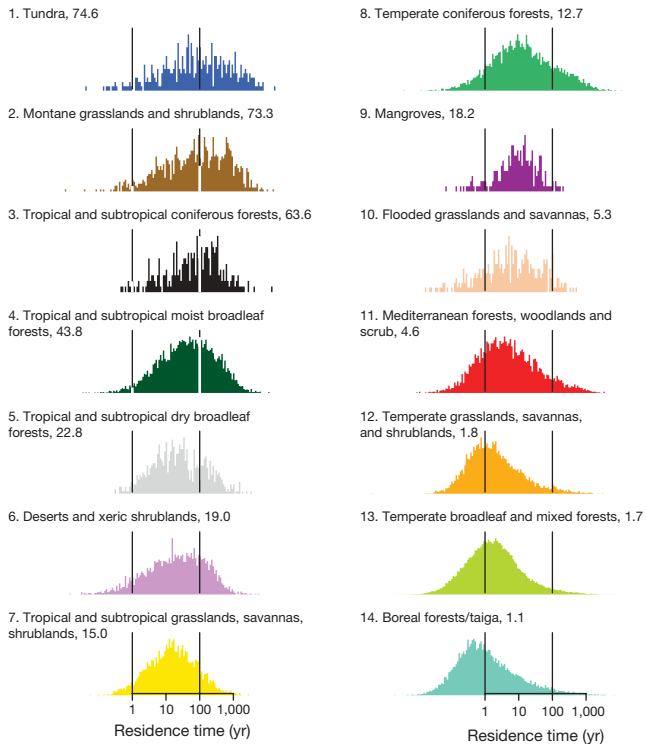

Figure 4 | Climate residence time (yr) in protected areas. Histograms represent the ratio of protected area diameter (km) to climate velocity (km h^{-1}), and are ordered by decreasing mean residence time across biomes. The vertical bar indicates 1 and 100 years.

©2009 Macmillan Publishers Limited. All rights reserved

Materials). Furthermore, we note the instantaneous velocity is sensitive to the grain of the analysis and the size of the kernels used to compute spatial and temporal gradients[17]. Throughout this study, we use a ~1 km spatial grain size, the finest available for global mean annual temperature, and a 9 grid cell spatial kernel, standard for creating gridded slopes from digital elevation models. We chose the fine spatial grain because both yearly dispersal capabilities for many species and large temperature changes often occur on the order of a few kilometres. In some cases, even finer resolution responses on the scale of metres may be sufficient to offset climate change as populations move from south to north facing slopes within a habitat[18].

Third, our index estimates the velocities and residence times of climates, not species. We make no assumptions about the tolerances of individual species. Implications for individual species depend on the breadth of tolerance[15], and our velocities apply to range edges, ecotones[19] and other features that reflect climate isoclines. For species with small tolerances, the velocity estimates closely approximate migration speeds required to potentially avoid extinction. For species with large tolerances, the residence times are underestimates. We also note that species do not move at constant rates[20] and, in some instances, the velocity of movements downhill may differ from those uphill; similarly leading-edge expansion and trailing-edge contraction will be different, reflecting the contrasting mechanisms. As a result of these caveats, we interpret these velocities as a relative index of the speeds required to keep pace with climate change rather than a calibrated index of migration rates.

It is, however, interesting to compare the magnitude and spatial patterns of the velocities with migration rate studies. A previous study[21] calculated the minimum distances between modelled current and future biomes from two Global Vegetation Models (GVMs) and interpreted them as necessary speeds for species migration. The study used similar emissions and temporal scales, a much coarser spatial grain (0.5 °C), and projections from an older generation of global climate models than those explored here. Accounting for uncertainty, the probability density function of our velocities are the same as those found previously[21]. For example, we calculated that 28.8% (0.5–66.9) of the globe had migration rates greater than 1 km yr^{-1}, compared with 17.4% and 21.1% from the two GVMs used previously[21]. These similarities are interesting given the many differences in the approaches used to explore migration rates (see Supplementary Material for further comparisons).

The rate of northward tree migration during the Holocene is estimated at about 1 km yr^{-1} after the last glacial maximum in Europe and North America[9]. The apparent paradox of such a fast migration rate relative to the limitations on plant dispersal[22] is possible by rare long-distance migration events[23] or high latitude refugia reseeding the landscape[24]. The latter means that post-glacial re-colonization velocities may have been as much as an order of magnitude slower than previously thought (~0.1 km yr^{-1}).

We project that large areas of the globe (28.8%) will require velocities faster than the more optimistic plant migration estimates from a landscape before anthropogenic fragmentation. Velocities on montane landscapes, in contrast, may fall within historic rates. The ability of complex topography to provide a spatial buffer for climate change has been recognized qualitatively[25] and evaluated over small geographic areas[26], but was muted in previous, coarser scale global analyses[21]. Considering these factors adds an important dimension to management strategies for addressing climate change, highlighting the greater vulnerability of large, extensive areas such as the lowland tropics and desert regions. In landscapes where small velocities are required, moderate-sized protected areas may be able to contain moving climates and ecosystems. Elsewhere, further steps must be taken. These include slowing the temporal gradient of climate change through reduced emissions, increasing the ability of plants and animals to disperse through managed relocation[7], or increasing the size of protected areas through habitat corridors and new reserves[6].

METHODS SUMMARY

In brief, for current climate, we used the 30-arcsec WorldClim Version 1.4 Annual Mean Temperature and Total Annual Precipitation bioclimatic variable[27]. Spatial gradients were calculated from a 3×3 grid cell neighbourhood using the average maximum technique[28] modified to accommodate different cell widths at different latitudes. Future temperature projections for each emissions scenario were averages of 16 global climate models statistically downscaled to 0.5 °C[29]. We computed temporal gradients as the slope of a linear model fit through each year of the time period of interest. Velocity is the ratio of the temporal gradient to the spatial gradient, and log transformed for visualization due to a highly skewed distribution. We report geometric means of the velocity to accommodate this skew. We compiled biomes from the World Wildlife Fund (WWF) Terrestrial Ecoregions[30] and protected areas from the World Database on Protected Areas (WDPA) Annual Release 2009 (web download version), February 2009. For each protected area centroid we sampled the velocity and biome to compare with estimates of reserve diameter. We discuss precipitation and uncertainty propagation in the Methods.

Full Methods and any associated references are available in the online version of the paper at www.nature.com/nature.

Received 27 August; accepted 3 November 2009.

1. Parmesan, C. & Yohe, G. A globally coherent fingerprint of climate change impacts across natural systems. *Nature* **421,** 37–42 (2003).
2. Nogués-Bravo, D., Araujo, M. B., Errea, M. P. & Martinez-Rica, J. P. Exposure of global mountain systems to climate warming during the 21st Century. *Glob. Environ. Change* **17,** 420–428 (2007).
3. Colwell, R. K., Brehm, G., Cardelus, C. L., Gilman, A. C. & Longino, J. T. Global warming, elevational range shifts, and lowland biotic attrition in the wet tropics. *Science* **322,** 258–261 (2008).
4. Thuiller, W., Lavorel, S., Araújo, M. B., Sykes, M. T. & Prentice, I. C. Climate change threats to plant diversity in Europe. *Proc. Natl Acad. Sci. USA* **102,** 8245–8250 (2005).
5. Loarie, S. R. *et al.* Climate change and the future of California's endemic flora. *PLoS One* **3,** e2502 (2008).
6. Hannah, L. Protected areas and climate change. *Ann. NY Acad. Sci.* **1134,** 201–212 (2008).
7. Hoegh-Guldberg, O. *et al.* Assisted colonization and rapid climate change. *Science* **321,** 345–346 (2008).
8. Williams, J. W., Jackson, S. T. & Kutzbach, J. E. Projected distributions of novel and disappearing climates by 2100 AD. *Proc. Natl Acad. Sci. USA* **104,** 5738–5742 (2007).
9. Pearson, R. G. Climate change and the migration capacity of species. *Trends Ecol. Evol.* **21,** 111–113 (2006).
10. Damschen, E. I., Haddad, N. M., Orrock, J. L., Tewksbury, J. J. & Levey, D. J. Corridors increase plant species richness at large scales. *Science* **313,** 1284–1286 (2006).
11. Joppa, L. N., Loarie, S. R. & Pimm, S. L. On the protection of "protected areas". *Proc. Natl Acad. Sci. USA* **105,** 6673–6678 (2008).
12. Murphy, J. M. *et al.* Quantification of modelling uncertainties in a large ensemble of climate change simulations. *Nature* **430,** 768–772 (2004).
13. Moritz, C. *et al.* Impact of a century of climate change on small-mammal communities in Yosemite National Park, USA. *Science* **322,** 261–264 (2008).
14. Kelly, A. E. & Goulden, M. L. Rapid shifts in plant distribution with recent climate change. *Proc. Natl Acad. Sci. USA* **105,** 11823–11826 (2008).
15. Parmesan, C. Ecological and evolutionary responses to recent climate change. *Annu. Rev. Ecol. Evol. Syst.* **37,** 637–669 (2006).
16. Lenoir, J., Gegout, J. C., Marquet, P. A., De Ruffray, P. & Brisse, H. A significant upward shift in plant species optimum elevation during the 20th century. *Science* **320,** 1768–1771 (2008).
17. Trivedi, M. R., Berry, P. M., Morecroft, M. D. & Dawson, T. P. Spatial scale affects bioclimate model projections of climate change impacts on mountain plants. *Glob. Change Biol.* **14,** 1089–1103 (2008).
18. Weiss, S. B., Murphy, D. D. & White, R. R. Sun, slope, and butterflies: topographic determinants of habitat quality for *Euphydryas editha*. *Ecology* **69,** 1486–1496 (1988).
19. Beckage, B. *et al.* A rapid upward shift of a forest ecotone during 40 years of warming in the Green Mountains of Vermont. *Proc. Natl Acad. Sci. USA* **105,** 4197–4202 (2008).
20. Van Houtan, K. S., Pimm, S. L., Halley, J. M., Bierregaard, R. O. & Lovejoy, T. E. Dispersal of Amazonian birds in continuous and fragmented forest. *Ecol. Lett.* **10,** 219–229 (2007).
21. Malcolm, J. R., Markham, A., Neilson, R. P. & Garaci, M. Estimated migration rates under scenarios of global climate change. *J. Biogeogr.* **29,** 835–849 (2002).
22. Clark, J. S. *et al.* Reid's paradox of rapid plant migration. *Bioscience* **48,** 13–24 (1998).
23. Clark, J. S. Why trees migrate so fast: confronting theory with dispersal biology and the paleorecord. *Am. Nat.* **152,** 204–224 (1998).

©2009 Macmillan Publishers Limited. All rights reserved

24. McLachlan, J. S., Clark, J. S. & Manos, P. S. Molecular indicators of tree migration capacity under rapid climate change. *Ecology* **86,** 2088–2098 (2005).
25. Peterson, D. L., Schreiner, E. G. & Buckingham, N. M. Gradients, vegetation and climate: spatial and temporal dynamics in the Olympic Mountains, USA. *Glob. Ecol. Biogeogr. Lett.* **6,** 7–17 (1997).
26. Peterson, A. T. Projected climate change effects on Rocky Mountain and Great Plains birds: generalities of biodiversity consequences. *Glob. Change Biol.* **9,** 647–655 (2003).
27. Hijmans, R. J., Cameron, S. E., Parra, J. L., Jones, P. G. & Jarvis, A. Very high resolution interpolated climate surfaces for global land areas. *Int. J. Climatol.* **25,** 1965–1978 (2005).
28. Burrough, P. A. & McDonnell, R. A. *Principles of GIS* 190 (Oxford Univ. Press, 1998).
29. Maurer, E. P., Adam, J. C. & Wood, A. W. Climate model based consensus on the hydrologic impacts of climate change to the Rio Lempa basin of Central America. *Hydrol. Earth Syst. Sci.* **13,** 183–194 (2009).
30. Olson, D. M. *et al.* Terrestrial ecoregions of the world: a new map of life on earth. *Bioscience* **51,** 933–938 (2001).

Supplementary Information is linked to the online version of the paper at www.nature.com/nature.

Acknowledgements This work was made possible through the support of the Gordon and Betty Moore Foundation and the Stanford University Global Climate and Energy Project.

Author Contributions D.D.A. conceived the study. S.R.L., D.D.A., P.B.D., H.H. and C.B.F. designed the study. S.R.L., P.B.D. and G.P.A. performed the analysis. S.R.L., D.D.A., P.B.D., C.B.F., H.H. and G.P.A. wrote the paper.

Author Information Reprints and permissions information is available at www.nature.com/reprints. Correspondence and requests for materials should be addressed to S.R.L. (loarie@stanford.edu).

©2009 Macmillan Publishers Limited. All rights reserved

METHODS

Temporal gradients. We performed all analyses using both mean annual temperature (°C) and total annual precipitation (mm). Future temperature and precipitation projections for each emissions scenario were averages of 16 GCMs statistically downscaled to 0.5 °C[29]. Exactly one ensemble member was used from each GCM (Supplementary Table 1).

To compute temporal gradients, we first summarized the 16 GCM time series for each pixel (for a given emission scenario) into mean, upper and lower time series by calculating the mean and the mean ± 1 s.d. of the 16 projections at each year in the time series (Supplementary Fig. 1, dashed black lines and grey bounds). We then calculated the mean slope and intercept from this mean time series using linear regression (Supplementary Fig. 1, solid black line). Next, we approximated upper and lower slopes as the difference between the height of the mean regression line at 2000 and the height of the upper and lower time series at 2100 divided by 101 years (Supplementary Fig. 1, red and blue lines).

We summarize uncertainty by mapping these upper and lower gradients globally for temperature (Supplementary Fig. 2) and precipitation (Supplementary Fig. 3). We plot their histograms (Supplementary Figs 4 and 5) grouped by biome. Biomes were compiled from the WWF Terrestrial Ecoregions[30]. Interestingly, because in many places the mean change in precipitation is close to zero but the uncertainty is large, in many cases both the upper and lower uncertainty bounds on the precipitation temporal gradients are larger than the mean.

There are several different approaches that could be used to estimate temporal gradients. One alternative approach would be to first calculate separate slopes for each pixel from each of the 16 separate GCM time series and subsequently calculate the mean and s.d. from these 16 slopes. To explore whether selecting this alternative approach would influence estimates of temporal gradients and uncertainty, we compared both approaches for a single arbitrary pixel in California (Supplementary Fig. 6). In the graph illustrating the alternative approach (Supplementary Fig. 6, right column), we arbitrarily fix the height of the upper and lower lines in the year 2000 to the height of the mean line. For the pixel in Supplementary Fig. 6, under the SRES A1B emission scenario simulations from 2000–2100, the two approaches yield similar results with a temperature temporal gradient of 0.03 °C yr^{-1} (0.02–0.04) for both approaches, and a precipitation temporal gradient of 0.14 (1.66–2.69) for the approach used here and 0.14 mm yr^{-1} (1.20–1.48) for the alternative approach.

Next, we explored whether the global land surface distribution of temporal gradients was influenced by the approach used. Supplementary Fig. 7 shows global land surface histograms of the mean (black), lower (blue) and upper (red) temporal gradient estimates for temperature and precipitation calculated from each of the two approaches under the SRES A1B emission scenario simulations from 2000–2100. The global results are very similar regardless of the approach used with average temperature temporal gradients of 0.04 °C yr^{-1} (0.03–0.05) for either approach, and average precipitation temporal gradients of 0.59 mm yr^{-1} (0.62–1.72) for the approach used here and 0.55 mm yr^{-1} (0.54–1.06) for the alternative approach. We chose the approach used here because we found it easier to visualize.

Spatial gradients. We performed all analyses globally at 30 arcsec (~0.8 km). We used the 30-arcsec WorldClim Version 1.4 (ref. 27) Annual Mean Temperature and Annual Total Precipitation bioclimatic variables[27] compiled from 1950–2000 to approximate current climate. To decrease the incidence of flat spatial gradients that cause infinite speeds, we added uniformly distributed random noise from −0.05 to 0.05 °C, or from −0.5 to 0.5 mm, to each pixel for temperature and precipitation, respectively.

From the current climate maps, we calculated spatial gradients from a 3×3 grid cell neighbourhood using the average maximum technique[28] modified to accommodate different cell widths at different latitudes. To convert cell height in latitudinal degrees to km, we used 111.325 km $degree^{-1}$. To convert cell width in longitudinal degrees to km we calculated $\cos\left(\frac{\pi}{180}y\right)111.325$, in which y is the latitude of the pixel in degrees.

Uncertainty in WorldClim temperature and precipitation varies spatially but is around 0.1 °C and 10 mm^3. Using the analogous PRISM dataset[31] over the western United States as a reference (Supplementary Fig. 8), we determined the difference between WorldClim and PRISM to be similar to the reported uncertainty. Propagating uncertainty in WorldClim through to the spatial gradient would overestimate the uncertainty because the spatial gradient is derived from relative climate and not absolute magnitudes (Supplementary Fig. 9). Accordingly, we estimate uncertainty in the spatial gradient directly. First, we note that standard deviation of spatial gradients within WorldClim varies by topographic Digital Elevation Model (DEM) slope. To accommodate this, we calculate empirical standard deviations binned by topographic slope and fit a smoothed spline through them (Supplementary Fig. 10, green lines). We divided the log of topographic slope (m km^{-1}) into bins of size 0.1, in which each bin, j, contained I_j pixels. Because the topographic slope is an input into the WorldClim model, these standard deviations may underestimate actual uncertainty in the spatial gradient. Instead, we use PRISM as a reference and calculate the s.d. for each bin as

$$\sigma_j = \sqrt{\frac{1}{I_j - 1}\sum_{i=1}^{I_j}(W_{j,i} - P_{j,i})^2}$$

between the WorldClim spatial gradient, $W_{j,i}$, and the paired PRISM, $P_{j,i}$, spatial gradient at each pixel, i, in each bin, j. We use the smoothed spline fit through these estimates as the one standard deviation upper and lower uncertainty bounds on the spatial gradient (Supplementary Fig. 10, red and blue lines). We map this uncertainty globally for temperature (Supplementary Fig. 11) and precipitation (Supplementary Fig. 12). We note that although we apply uncertainty derived from the western United States across the globe, weather station density is lower in less developed countries. This means that uncertainty is probably higher in such countries especially if they are mountainous. The development of higher accuracy global weather surfaces with known uncertainties is a priority for better understanding the impact of climate change on ecosystems.

Velocity calculations. To combine the 0.5 °C (~50 km) temporal gradient maps with the 1 km spatial gradient maps, we resampled the temporal gradient maps to 1 km. We calculated speed as the ratio of the temporal gradient to the spatial gradient. We only computed speed in cells with data on both spatial and temporal gradients. This excluded certain areas along the coast that were not included in the 0.5 °C maps.

To estimate uncertainty in the velocity calculations, we propagated the upper and lower uncertainty in the temporal and spatial gradients. Again, we map this uncertainty globally for temperature (Supplementary Fig. 13) and precipitation (Supplementary Fig. 14), and plot their histograms grouped by biome (Supplementary Figs 15 and 16). For visualization, we log transformed the histograms due to a highly skewed distribution. In the manuscript text, we report geometric means of the speed index to accommodate this skew. Infinite speeds (resulting from a spatial gradient of zero) were set to the global finite 99.99% quantile value for the purposes of plotting.

We recognize that combining gradients with different measurement scales and units (spatial and temporal) into a single index raises several uncertainties and possible issues. First, as we state in the manuscript, the kernels used to produce gradients are arbitrary and cannot be made directly equivalent. We use temporal gradients from 2000–2100 but explore gradients from 2000–2050 and 2050–2100. We use the finest spatial gradient possible globally—a grid of 9 grid cells—based on our argument of the potential important role of microclimates. Second, extrapolating these velocities over time or space must be done with caution, as doing so assumes that the gradients extrapolate linearly. In reality, topography can change suddenly as plains give way to mountains and vice versa. Likewise, depending on emission scenarios and climate feedbacks, climate change will probably not proceed linearly over the next century. We have purposely left differences in emission scenarios out of our uncertainty analysis (as opposed to differences in global climate models) because future climate policy will give society varying degrees of control over future emissions.

We repeated the analyses of the velocity of temperature change (km yr^{-1}) using the 2050–2100 SRES B1 and SRES A2 emissions scenario temporal gradient (Supplementary Fig. 17). Increasing emissions from the milder B1 to the more severe A2 scenario increases mean velocities from 0.28 to 0.57 km yr^{-1}.

To explore the relationship between topographic slope and the velocity of climate change, we plotted the speed (km yr^{-1}) of temperature and precipitation change by topographic slope (m km^{-1}) using the WorldClim DEM[27] and computed the correlation (Supplementary Fig. 18). Red points are speeds of temperature change for each pixel (correlation coefficient = −0.92). Black points are speeds of precipitation change (correlation coefficient = −0.46). The correlation is stronger for temperature.

We map areas where the speed from precipitation change is greater than the speed from temperature change as well as the average magnitude of climate change velocity from temperature and precipitation (Supplementary Fig. 19). This combined metric does not include the relative directions of these components.

Residence time. The WDPA is a joint product of the United Nations Environment Programme (UNEP) and International Union for Conservation of Nature (IUCN), prepared by the UNEP World Conservation Monitoring Centre (UNEP-WCMC), supported by the IUCN World Commission on Protected Areas (WCPA) and working with governments, the secretariats of multilateral environmental agreements and collaborating non-governmental organizations. For further information, contact protectedareas@unep-wcmc.org. This database lists centroid coordinates and areas for most protected areas. We used the Geographic Information System (GIS) area field only if documented area

©2009 Macmillan Publishers Limited. All rights reserved

field was blank. For each protected area centroid we sampled the speed and biome to compare with protected area size. We define protected area size as the diameter of a circle of equivalent area to the protected area centred on the centroid of the protected area. This assumes that the protected areas are circular and disconnected. The circular assumption would only be violated if the protected areas had systematically different aspect ratios and orientations by biome. Although some protected areas are not disconnected, we assume that this is a small overall proportion of protected areas.

We plotted histograms of reserve size (km) by biome using biomes from the WWF Terrestrial Ecoregions[30] and centroids of 126,068 protected areas from the WDPA (Supplementary Fig. 20). We assumed reserves were circular and disconnected and computed diameters from their areas. We use these diameters as estimates of reserve size in kilometres.

To estimate uncertainty in the residence time calculations, we propagate the upper and lower uncertainty in the velocity calculations. As before, we plot the histograms of residence time grouped by biome (Supplementary Figs 21 and 22). We log transformed the histograms and report geometric means in the manuscript text to accommodate the skewed protected area size data and residence time distributions.

Comparisons with migration rate studies. The probability distribution function of our temperature-based velocities are consistent with those described previously[21] when uncertainty is accounted for (Supplementary Table 2). We also map the speed of temperature change (km yr^{-1}) by latitude and compare these values to speeds calculated previously[21] using the Biome3 and MAPSS global vegetation models (Supplementary Fig. 23). Velocities reported previously[21] peak in the high latitudes as opposed to the lower latitudes as found in this study. There are many differences in the approaches used that may account for this contrast. A fundamental difference is that velocities here are based purely on climate gradients, whereas those reported previously are based on the distances between modelled present and future biomes. The approach used previously results in velocities being sensitive to biome size. Another key difference is the much finer spatial resolution of our analysis, which emphasizes the importance of topographic variability. The latter may partially drive the differences in the latitudinal distribution. In this study, higher velocities in lower latitudes are largely driven by the dominance of flat areas (the Amazon Basin and the Sahara, for example) relative to the dominance of steeper topography (and thus lower velocities) in the higher latitudes. The coarser resolution used previously[23] mutes the influence of fine scale topographic variability, contributing to a different latitudinal distribution of climate velocity.

All analyses were performed in R.

31. Daly, C. *et al.* Physiographically sensitive mapping of climatological temperature and precipitation across the conterminous United States. *Int. J. Climatol.* **28**, 2031–2064 (2008).

©2009 Macmillan Publishers Limited. All rights reserved